ChemComm

Eutectic melt crystallization of L10-FePt

Journal:	*ChemComm*
Manuscript ID	CC-COM-10-2018-008199.R1
Article Type:	Communication

Journal Name

COMMUNICATION

Eutectic melt crystallization of $L1_0$-FePt

Jingming Zhang, Changning Li, Jason Armstrong, Shenqiang Ren*

Received 00th January 20xx,
Accepted 00th January 20xx

DOI: 10.1039/x0xx00000x

www.rsc.org/

Here, we report the eutectic growth control of the ordered $L1_0$-FePt, which directs the nucleation, growth and crystallization of FePt sheets in a single-step reaction. The nature of eutectic crystallization at the eutectic point suggests its role as a high-temperature solvent, exhibiting the advantage in scale-up production of metastable alloys.

To date, colloidal metal nanoparticles through liquid phase growth are dominated by using organic solvents[1-4]. However, the boiling point of organic solvents, ranging from 473 K to 623 K, is usually far low the disorder-order transition temperature[5, 6]. Therefore, a consequential thermal annealing at a higher temperature is indispensable to initiate phase transformation for the ordered phase, which however induces the nanoparticle aggregation for a size beyond the single-domain region[7]. Therefore, a single-step high-temperature reaction for the nanostructured alloy phase is highly desirable, particularly its metastable form. Eutectic reaction addresses all these challenges by its high-temperature reaction limit of more than 1655 K, corresponding to the boiling point. The eutectic composition describes its melting point at which temperature the mixed substances become fully molten at a single temperature[8]. The solid microstructures developed from eutectic reactions in complex material systems depend on several factors, such as the reaction and phase transformation temperature, and the interfacial nucleation from solid solutions[9-10]. Therefore, the understanding of eutectic reaction could offer a great potential to elucidate the chemical and physical mechanisms underlying the eutectic-induced dynamic metastable phase transformation[5, 12, 13].

Department of Mechanical and Aerospace Engineering, and Research and Education in Energy, Environment & Water (RENEW) Institute, University at Buffalo, The State University of New York, Buffalo, NY 14260.
** Email: shenren@buffalo.edu*
Electronic Supplementary Information (ESI) available: sample preparation and additional structural characterization. See DOI: 10.1039/x0xx00000x

Here, we report the eutectic reaction and crystallization control of $L1_0$-ordered FePt phase. The $L1_0$-FePt is selected as the prototypical example material due to its unique physicochemical properties, such as high magnetocrystalline anisotropy, surface-active catalytic sites using compositional tuning, and high energy density, which show great potentials for a variety of applications in energy-critical systems[14-17]. It is fundamentally important to examine how eutectic reaction and phase transformation coexist for understanding the disorder-order transitions in FePt phase. Furthermore, the reaction temperature and the stoichiometry effects on the magnetic energy product of $L1_0$-FePt is investigated. The eutectic salt melt reaction enables the ordered $L1_0$ phase of FePt nanoparticles with an average diameter of 20 nanometers, and the entire synthesis occurs in one-pot and one single-step, with no further heat treatment needed after the initial reaction.

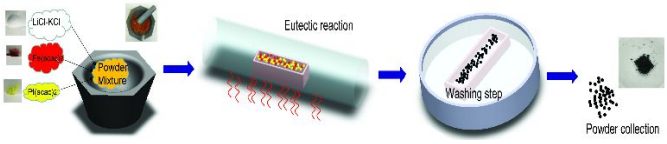

Figure 1. Eutectic salt melt synthesis and crystallization of $L1_0$ FePt.

The overall scheme of eutectic salt melt reaction method for $L1_0$-FePt growth is presented in Figure 1. The LiCl-KCl eutectic composition with 50 wt. % of KCl is selected in the synthesis of $L1_0$ FePt nanoparticles, which shows its eutectic point of 620 K and can go as high as 1273 K. The 10:1 mass ratio between the eutectic salt and Fe and Pt precursors is mixed vigorously in an agate mortal. The powder mixture is then transferred into an alumina crucible and sintered in the furnace. After reaching the eutectic point of LiCl-KCl at 626 K, the LiCl-KCl eutectic salt is melted and serves as the high-temperature solvent. Compared to the traditional organic solvent synthesis, the window of reaction temperature is broader and higher using the LiCl-KCl eutectic salts. Under the reaction temperature of

823 K, $L1_0$ FePt can be created in one single step and one pot. High purity product could be obtained by this method since the LiCl-KCl eutectic salts could be removed after the reaction by washing the product with the deionized water in a short time. After all the eutectic salts are dissolved in the DI water, the black powder product is collected and dried for further analysis.

Flake-shape FePt nanostructures are obtained in one-pot and single-step, where this unique flake-shape FePt could be a result of the lamellar structure formed during the solidification of the eutectic salts within the cooling process[18]. Figures 2a-b show the SEM image and EDS mapping of the elemental distribution of Fe and Pt. In which, Fe element were represented by red colour and Pt element were represented by green colour. No signs of phase separation are observed, while the elemental analysis shows 1 Fe: 1 Pt, validating the FePt stoichiometry in the product (The details are shown in supporting information). It should be noted that the stoichiometries of FePt can be controlled by tuning the ratio of different amounts of Fe and Pt precursors used in the reaction. Figure 2c presents the TEM image of as-synthesized FePt with the average size of 20 nm by the eutectic salt, suggesting that the flake shape powders are assembled from $L1_0$-FePt nanoparticles. The TEM image further confirms that the LiCl-KCl eutectic salt melt crystallization method is adequate to produce small diameter FePt nanoparticles and prevents the sintering induced aggregation. The x-ray diffraction (XRD) spectrum is presented to resolve the (001) and (110) planes in Figure 2d for 923K and 1023K synthesized sample, which confirms the formation of highly ordered $L1_0$ phase FePt nanoparticles through the eutectic salt melt and crystallization method. In addition, the peak separation of (200) and (002) is another indicator to confirm the formation of $L1_0$-FePt phase at these temperatures; while at 723K, the peaks for (200) and (002) are joined together indicating the formed FePt sample are in FCC phase. No signals from LiCl or KCl crystals was observed from the XRD data, which indicates a high purity of FePt sample is prepared by this method.

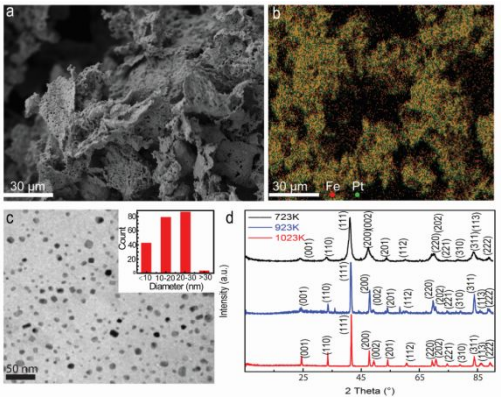

Figure 2. (a) The scanning electron microscopy (SEM) image of FePt; (b) The EDS elemental mapping of FePt powder; (c) TEM image of $L1_0$-FePt nanoparticles; and (d) The XRD spectra of $L1_0$-FePt sintered at 723K, 923 K and 1,023 K, respectively.

Figure 3 shows the magnetic hysteresis loops of $L1_0$-FePt synthesized under different reaction temperatures of 823 K, 923 K, and 1,023 K. The stoichiometry dependence in FePt is also synthesized at 1,023 K. The coercivity is dependent on the eutectic reaction temperature. The coercivity is increased from 4 KOe to 8 KOe by increasing the reaction temperature from 823 K to 923 K. The coercivity is further enhanced by increasing the reaction temperature to 1,023K, which shows the highest coercivity of 16 KOe. The increased coercivity indicates the improved crystallinity of $L1_0$-FePt under the increased reaction temperature. For the stoichiometry dependent investigation, the increased amount of Fe led to an increased saturation magnetization, while the increased amount of Pt in the product led to the kinks in the hysteresis loop due to the presence of non-magnetic Pt. At the stoichiometry of $L1_0$-FePt phase, the largest coercivity is obtained at 16 KOe, with a relatively high value of saturation magnetization of 33.6 emu/g[6, 7, 15, 19].

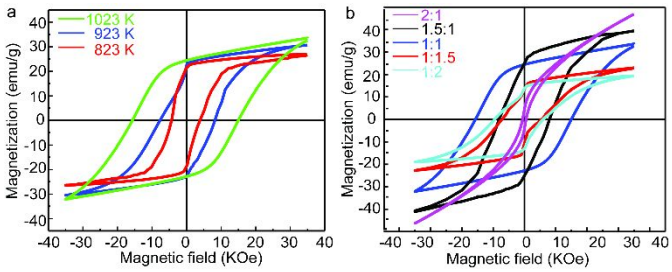

Figure 3. (a-b) Magnetic hysteresis loops of $L1_0$-FePt sintered at different temperatures, and with the Fe:Pt stoichiometry dependence, respectively.

The stoichiometry $L1_0$ FePt phase exhibits a high coercivity. However, a high magnetic energy product material requires both high coercivity and a large saturation magnetization. Therefore, a magnetically semi-hard coating (cobalt) onto the $L1_0$-FePt would increase the saturation magnetization while maintaining its coercivity[20]. Figure 4 illustrates the morphology and magnetic behaviours of the cobalt coated FePt sample (FePt-Co). Both the eutectic salt melt and traditional liquid phase synthesis method are investigated for the cobalt coating. However, magnetic hysteresis loop shows the kink behaviour using the eutectic salt melt synthesis method. Therefore, in the following, we utilize the solution assembly induced FePt-Co phase to investigate the exchange coupling effect on the energy product. From the EDS elemental mapping (Fig. 4b), the cobalt is evenly dispersed in the product. In the EDS mapping, Fe is represented in red, Co is represented in purple, and Pt is represented in green. The saturation magnetization would increase based on the amount of cobalt in the product. However, the coercivity of the final product would be reduced by the semi-hard magnetic cobalt at the same time. Therefore, the amount of cobalt is essential to optimize the energy product performance of FePt-Co magnets. As increasing the amount of cobalt from 10 wt. % to 15 wt. %, the saturation magnetization is significantly increased from 44.5 emu/g to 49.69 emu/g, while the coercivity is reduced from 16 KOe to 13 KOe. The saturation

magnetization of FePt-Co could be further increased by adding more cobalt composition, however, the kink becomes pronounced to further reduce the magnetic energy product. The magnetic energy product BH_{max} is shown in Figure 4d The BH_{max} for $L1_0$-FePt powder synthesized at 1,023 K is 4.4 MGOe. The BH_{max} can be significantly affected by the cobalt coating. When the mass ratio of the cobalt is less than 15 wt. %, no significant improvement in the BH_{max} is shown by the cobalt coating. For an increased amount of cobalt, the BH_{max} shows an increasing trend with 16% improvement in energy product for 5 MGOe at 15 wt. % cobalt coating. Further increasing the amount of cobalt to 25 wt. % decreases the magnetic energy product to 3.7 MGOe, because the increased saturation magnetization cannot compensate for the significant loss of coercivity. It should also be noted that the cobalt coated sample is not fully saturated under an external field of 6 T. The magnetic performance will be even better if a higher field is applied.

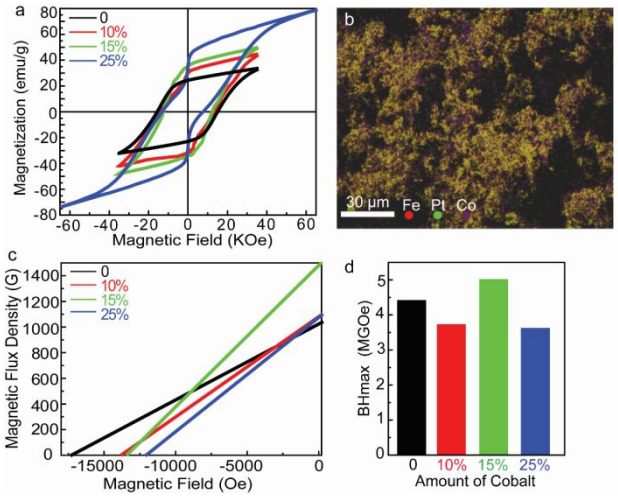

Figure 4. (a) Magnetic hysteresis loops of $L1_0$-FePt-Co powders at different Co coating concentrations; (b) The EDS elemental mapping of the FePt-Co product; (c) The B-H plot of FePt-Co magnets at different Co coating concentrations; (d) The energy product (BH_{max}) of FePt-Co magnets.

The eutectic salt melt and crystallization method is shown to be an efficient and single-step method to prepare $L1_0$-FePt phase with an average diameter of 20 nm. The as-synthesized $L1_0$-FePt particles exhibit a coercivity of 16 KOe and a saturation magnetization of 33.6 emu/g. The magnetic behaviour can be further improved by cobalt coating for the formation of FePt-Co structures, while the optimum magnetic energy product obtained is 5.0 MGOe. The eutectic salt melt method shows great potential in synthesized metastable magnetic metal materials.

Conflicts of interest

There are no conflicts to declare.

Acknowledgements

S.R. acknowledges the support from the U.S. National Science Foundation (NSF) under the CAREER Award No: NSF-DMR-1830749.

Notes and references

1. A. H. Lu, E. L. Salabas and F. Schuth, *Angew Chem Int Ed Engl*, 2007, **46**, 1222-1244.
2. N. A. Frey, S. Peng, K. Cheng and S. Sun, *Chem Soc Rev*, 2009, **38**, 2532-2542.
3. W. Lei, Y. Yu, W. Yang, M. Feng and H. Li, *Nanoscale*, 2017,**9**, 12855-12861.
4. Y. Yu, P. Mukherjee, Y. Tian, X. -Z. Li, J. E. Shield and D. J. Sellmyer, *Nanoscale* 2014, **6**, 12050-12055.
5. X. Liu, N. Fechler and M. Antonietti, *Chem Soc Rev*, 2013, **42**, 8237-8265.
6. S. Sun, C. B. Murray, D. Weller, L. Folks and A. Moser, *Science*, 2000, **287**, 1989-1992.
7. M. Chen, J. P. Liu and S. Sun, *Journal of the American Chemical Society*, 2004, **126**, 8394-8395.
8. A. S. Basin, A. B. Kaplun, A. B. Meshalkin and N. F. Uvarov, *Russian Journal of Inorganic Chemistry*, 2008, **53**, 1509-1511.
9. W. Lei, D. Portehault, R. Dimova and M. Antonietti, *J Am Chem Soc*, 2011, **133**, 7121-7127.
10. H.-L. Li, Z.-N. Du, G.-L. Wang and Y.-C. Zhang, *Materials Letters*, 2010, **64**, 431-434.
11. M. K. Rybarczyk, E. Gontarek, M. Lieder and M.-M. Titirici, *Applied Surface Science*, 2018, **435**, 543-551.
12. N. Dharuman and L. John Berchmans, *Ceramics International*, 2013, **39**, 8767-8771.
13. Y. n. Wei, Z. Liu, S. Ran, A. Xia, T.-F. Yi and Y. Ji, *Journal of Materials Research*, 2017, **32**, 883-889.
14. M. Andreas, T. Kentaro, T. M. David, A. Manfred, S. Yoshiaki, I. Yoshihiro, S. Shouheng and E. F. Eric, *Journal of Physics D: Applied Physics*, 2002, **35**, R157.
15. E. Fernandez, K. H. Tu, P. Ho and C. A. Ross, *Nanotechnology*, 2018, **29**, 465301.
16. S. Kurtz, E. Varga, M. J. Siddiq, M. Niemier, W. Porod, X. S. Hu and G. H. Bernstein, *Journal of Physics: Condensed Matter*, 2011, **23**, 053202.
17. J. Llandro, J. J. Palfreyman, A. Ionescu and C. H. Barnes, *Med Biol Eng Comput*, 2010, **48**, 977-998.
18. C. De Rosa, C. Park, E. L. Thomas and B. Lotz, *Nature*, 2000, **405**, 433.
19. D. Li, N. Poudyal, V. Nandwana, Z. Jin, K. Elkins and J. P. Liu, *Journal of Applied Physics*, 2006, **99**, 08E911.
20. W. Yang, W. Lei, Y. Yu, W. Zhu, T. George, X. –Z. Li, D. J. Sellmyer and S. Sun, *J. Mater. Chem. C*, 2015, **3**, 7075-7080.